Spectrochimica Acta Part A 81 (2011) 372–379

Contents lists available at ScienceDirect

Spectrochimica Acta Part A: Molecular and Biomolecular Spectroscopy

journal homepage: www.elsevier.com/locate/saa

Synthesis, X-ray crystal structure and fluorescent spectra of novel pyrazolo[1,5-*a*]pyrazin-4(5*H*)-one derivatives

Liang-Wen Zheng, Zhong-Liang Gong, Wen-Long Liu, Ying-Rui Liu, Bao-Xiang Zhao *

Institute of Organic Chemistry, School of Chemistry and Chemical Engineering, Shandong University, Jinan 250100, PR China

ARTICLE INFO

Article history:
Received 24 April 2011
Received in revised form 5 June 2011
Accepted 13 June 2011

Keywords:
Synthesis
Pyrazolopyrazine
X-ray crystal
UV–vis absorption
Fluorescence

ABSTRACT

A series of fluorescent compounds, containing pyrazolo[1,5-*a*]pyrazin-4(5*H*)-one moiety, were designed and synthesized from ethyl 1-(2-oxo-2-phenylethyl)-3-phenyl-1*H*-pyrazole-5-carboxylates. The structures of the compounds have been confirmed by IR, ^{1}H NMR, HRMS and X-ray crystal diffraction. The optical properties of the compounds were investigated by UV–vis absorption and fluorescence spectroscopy. The effect of pH on the UV–vis absorption of compound **2a** in methanol–H_2O solutions was studied and interpreted by theory calculation. The pK_a value of compound **2a** was determined by the absorption spectra.

1. Introduction

Pyrazine has two nitrogen atoms at the 1,4-positions of a 6-membered ring and can be anticipated to have many functionalities and reactivities in comparison with benzene analogues [1]. Pyrazines form an important class of analogues, which occupy a special role in natural and synthetic compounds [2,3]. Pyrazine derivatives are well known for their anticancer [4], antinociceptive [5], anti-mycobacterial [6], anti-inflammatory activities [7]. Furthermore, pyrazine derivatives have a chromophoric system and perform strong fluorescence. One of the typical example of pyrazine derivatives is coelenterazine [8] that was found and isolated from aequorin [9,10] and is widely used as a probe to monitor intracellular levels of free calcium [11]. In addition, pyrazine derivatives have application in the chemical industry and many other fields such as crystallography [12], nonlinear optical materials [13], metal-organic materials [14], food additives [15] and medicinal chemistry [16]. On the other hand, pyrazole derivatives constitute another important class of heterocyclic compounds regardless of scarcity in nature [17]. Over the last decade, pyrazole derivatives have attracted interest of many researchers, because of their biological activities such as anticancer [18], antiglaucoma [19], antimicrobial [20], antimycobacterial [21] and anti-inflammatory activities [22]. Pyrazole derivatives are also applied in photography and fluorescent sensor [23], nonlinear optical materials [24], dyes [25,26] and organic light emitting devices [27].

Considering chromophoric system of pyrazine and pyrazole moiety, we designed a pyrazole-fused pyrazine structure that should be expected to have more interesting optical properties. Herein, we would like to report the synthesis, crystal structure, characterization and optical properties of 2,6-diphenylpyrazolo[1,5-*a*]pyrazin-4(5*H*)-ones.

2. Materials and methods

2.1. General

All reactions were performed under dry nitrogen in oven-dried glassware. Melting points were measured with an XD-4 digital micro melting point apparatus and were uncorrected. Infrared spectra were recorded with an Avtar 370 FT-IR (Termo Nicolet) spectrophotometer as thin films between KBr plates. ^{1}H NMR spectra were performed on a Bruker Avance 400 spectrometer at 400 MHz at room temperature. HRMS spectrometric data were recorded using a LTQ Orbitrap Hybrid mass spectrograph at 70 eV. UV–vis spectra were determined on a U-4100 (Hitachi). Fluorescent measurements were obtained on a Perkin-Elmer LS-55 luminescence spectrophotometer. The fluorescence quantum yields (Φ_F) were measured using quinine sulfate (Φ_{ref} = 0.51 in 0.1 N H_2SO_4) as fluorescence standard [28]. All the reagents and solvents employed were commercially available analytical grade without further purification.

* Corresponding author. Tel.: +86 531 88366425; fax: +86 531 88564464.
E-mail addresses: bxzhao@sdu.edu.cn, sduzhao@hotmail.com (B.-X. Zhao).

1386-1425/$ – see front matter © 2011 Elsevier B.V. All rights reserved.
doi:10.1016/j.saa.2011.06.025

2.2. General procedure for the synthesis of compounds **2**

Ethyl 1-(2-oxo-2-phenylethyl)-3-phenyl-1*H*-pyrazole-5-carboxylate derivatives **1** (2.0 mmol) was dissolved in AcOH (15 ml), and then formamide (5 ml) was added. The mixture was stirred and heated to reflux for 3–7 h, until the TLC indicated the end of the reaction. After this time, the reaction mixture was cooled to room temperature. Precipitate was filtered and washed with ethanol (5 ml), aqueous solution of $NaHCO_3$ (10%, 2 × 6 ml) and water (10 ml). Compounds **2** were obtained in 77–94% yield with high-purity.

2.3. The characterization of compounds **2**

2.3.1. 2,6-Diphenylpyrazolo[1,5-a]pyrazin-4(5H)-one (**2a**)

White solid, yield 78%; mp 277–278 °C; IR (KBr, cm^{-1}): 3165–3040 (NH), 1641 (C=O); ^1H NMR (DMSO, 400 MHz) δ: 7.40 (t, 1H, J = 7.2 Hz, Ar–H), 7.46–7.52 (m, 5H, Ar–H), 7.56 (s, 1H, pyrazole–H), 7.79 (d, 2H, J = 8.2 Hz, Ar–H), 8.00 (d, 2H, J = 7.2 Hz, Ar–H), 8.12 (s, 1H, pyrazine–H), 11.59 (s, 1H, NH); HRMS ($C_{18}H_{14}N_3O$): calcd for $[M+H]^+$ 288.1137; found 288.1137.

2.3.2. 2-(4-Chlorophenyl)-6-phenylpyrazolo[1,5-a]pyrazin-4(5H)-one (**2b**)

White solid, yield 94%; mp 321–322 °C; IR (KBr, cm^{-1}): 3167–3048 (NH), 1673 (C=O); ^1H NMR (DMSO, 400 MHz) δ: 7.46–7.52 (m, 3H, Ar–H), 7.54 (d, 2H, J = 8.6 Hz, Ar–H), 7.61 (s, 1H, pyrazole–H), 7.78 (d, 2H, J = 8.4 Hz, Ar–H), 8.02 (d, 2H, J = 8.6 Hz, Ar–H), 8.13 (s, 1H, pyrazine–H), 11.65 (s, 1H, NH); HRMS ($C_{18}H_{13}ClN_3O$): calcd for $[M+H]^+$ 322.0747; found 322.0732.

2.3.3. 2-(4-Methoxyphenyl)-6-phenylpyrazolo[1,5-a]pyrazin-4(5H)-one (**2c**)

White solid, yield 85%; mp 275–276 °C; IR (KBr, cm^{-1}): 3164–3036 (NH), 1664 (C=O), 1610 (C=N); ^1H NMR (DMSO, 400 MHz) δ: 3.81 (s, 3H, OCH_3), 7.04 (d, 2H, J = 8.8 Hz, Ar–H), 7.46 (s, 1H, pyrazole–H), 7.47–7.49 (m, 3H, Ar–H), 7.77 (d, 2H, J = 7.3 Hz, Ar–H), 7.92 (d, 2H, J = 8.8 Hz, Ar–H), 8.09 (s, 1H, pyrazine–H), 11.55 (s, 1H, NH); HRMS ($C_{19}H_{16}N_3O_2$): calcd for $[M+H]^+$ 318.1243; found 318.1245.

2.3.4. 6-(4-Chlorophenyl)-2-phenylpyrazolo[1,5-a]pyrazin-4(5H)-one (**2d**)

White solid, yield 92%; mp 316–318 °C; IR (KBr, cm^{-1}): 3173–3028 (NH), 1697 (C=O); ^1H NMR (DMSO, 400 MHz) δ: 7.40 (t, 1H, J = 8.0 Hz, Ar–H), 7.48 (t, 2H, J = 8.0 Hz, Ar–H), 7.55 (d, 2H, J = 8.6 Hz, Ar–H), 7.56 (s, 1H, pyrazole–H), 7.81 (d, 2H, J = 8.6 Hz, Ar–H), 8.00 (d, 2H, J = 8.0 Hz, Ar–H), 8.17 (s, 1H, pyrazine–H), 11.72 (s, 1H, NH); HRMS ($C_{18}H_{13}ClN_3O$): calcd for $[M+H]^+$ 322.0747; found 322.0751.

2.3.5. 2,6-Bis(4-chlorophenyl)pyrazolo[1,5-a]pyrazin-4(5H)-one (**2e**)

Yellow solid, yield 91%; mp >330 °C; IR (KBr, cm^{-1}): 3156–3041 (NH), 1681 (C=O); ^1H NMR (DMSO, 400 MHz) δ: 7.55 (d, 2H, J = 8.4 Hz, Ar–H), 7.57 (d, 2H, J = 8.4 Hz, Ar–H), 7.62 (s, 1H, pyrazole–H), 7.80 (d, 2H, J = 8.4 Hz, Ar–H), 8.02 (d, 2H, J = 8.4 Hz, Ar–H), 8.18 (s, 1H, pyrazine–H), 11.70 (s, 1H, NH); HRMS ($C_{18}H_{12}Cl_2N_3O$): calcd for $[M+H]^+$ 356.0357; found 356.0346.

2.3.6. 6-(4-Chlorophenyl)-2-(4-methoxyphenyl)pyrazolo[1,5-a]pyrazin-4(5H)-one (**2f**)

White solid, yield 86%; mp 324–325 °C; IR (KBr, cm^{-1}): 3168–3041 (NH), 1642 (C=O), 1610 (C=N); ^1H NMR (DMSO, 400 MHz) δ: 3.81 (s, 3H, OCH_3), 7.03 (d, 2H, J = 8.8 Hz, Ar–H), 7.46 (s, 1H, pyrazole–H), 7.55 (d, 2H, J = 8.6 Hz, Ar–H), 7.80 (d, 2H, J = 8.6 Hz, Ar–H), 7.92 (d, 2H, J = 8.8 Hz, Ar–H), 8.14 (s, 1H, pyrazine–H), 11.59 (s, 1H, NH); HRMS ($C_{19}H_{15}ClN_3O_2$): calcd for $[M+H]^+$ 352.0853; found 352.0856.

2.3.7. 6-(4-Methoxyphenyl)-2-phenylpyrazolo[1,5-a]pyrazin-4(5H)-one (**2g**)

White solid, yield 77%; mp 307–308 °C; IR (KBr, cm^{-1}): 3167–3036 (NH), 1678 (C=O), 1607 (C=N); ^1H NMR (DMSO, 400 MHz) δ: 3.82 (s, 3H, OCH_3), 7.05 (d, 2H, J = 8.7 Hz, Ar–H), 7.39 (t, 1H, J = 7.7 Hz, Ar–H), 7.48 (t, 2H, J = 7.7 Hz, Ar–H), 7.53 (s, 1H, pyrazole–H), 7.73 (d, 2H, J = 8.7 Hz, Ar–H), 7.99 (d, 2H, J = 7.7 Hz, Ar–H), 8.04 (s, 1H, pyrazine–H), 11.50 (s, 1H, NH); HRMS ($C_{19}H_{16}N_3O_2$): calcd for $[M+H]^+$ 318.1243; found 318.1247.

2.3.8. 2-(4-Chlorophenyl)-6-(4-methoxyphenyl)pyrazolo[1,5-a]pyrazin-4(5H)-one (**2h**)

Yellow solid, yield 84%; mp 295–297 °C; IR (KBr, cm^{-1}): 3168–3045 (NH), 1673 (C=O), 1612 (C=N); ^1H NMR (DMSO, 400 MHz) δ: 3.82 (s, 3H, OCH_3), 7.05 (d, 2H, J = 8.8 Hz, Ar–H), 7.53 (d, 2H, J = 8.5 Hz, Ar–H), 7.56 (s, 1H, pyrazole–H), 7.72 (d, 2H, J = 8.8 Hz, Ar–H), 8.00 (d, 2H, J = 8.5 Hz, Ar–H), 8.02 (s, 1H, pyrazine–H), 11.54 (s, 1H, NH); HRMS ($C_{19}H_{15}ClN_3O_2$): calcd for $[M+H]^+$ 352.0853; found 352.0844.

2.3.9. 2,6-Bis(4-methoxyphenyl)pyrazolo[1,5-a]pyrazin-4(5H)-one (**2i**)

White solid, yield 85%; mp 305–307 °C; IR (KBr, cm^{-1}): 3162–3025 (NH), 1658 (C=O), 1613 (C=N); ^1H NMR (DMSO, 400 MHz) δ: 3.81 (s, 3H, OCH_3), 3.82 (s, 3H, OCH_3), 7.03 (d, 2H, J = 8.7 Hz, Ar–H), 7.04 (d, 2H, J = 8.7 Hz, Ar–H), 7.44 (s, 1H, pyrazole–H), 7.72 (d, 2H, J = 8.7 Hz, Ar–H), 7.92 (d, 2H, J = 8.7 Hz, Ar–H), 8.02 (s, 1H, pyrazine–H), 11.50 (s, 1H, NH); HRMS ($C_{20}H_{18}N_3O_3$): calcd for $[M+H]^+$ 348.1348; found 348.1349.

2.4. Crystallography

Suitable single crystals of **2c** for X-ray structural analysis were obtained by slow evaporation of ethanol solution. The X-ray diffraction measurement was carried out using a Bruker Smart CCD diffractometer. The structure was solved by direct methods with the SHELXS-97 program and refined by the full-matrix least squares method on F^2 data using the SHELXL-97 program [29]. PLATON program was used for the structure analysis [30]. Molecular graphics were drawn by ORTEP-3 for Windows. The crystal data and details concerning the data collection and structure refinement are given in Table 1.

CCDC 808752 (**2c**) contains the supplementary crystallographic data for this paper. These data can be obtained free of charge from The Director, CCDC, 12, Union Road, Cambridge, CB2 1EZ, UK (Fax: +44 1223 336033; e-mail: deposit@ccdc.cam.ac.uk or http://www.ccdc.cam.ac.uk).

Table 1
Summary of crystal data and structure refinement for compound **2c**.

Compound	**2c**
Empirical formula	$C_{19}H_{15}N_3O_2$
Formula weight	317.34
Crystal system	Monoclinic
Space group	$P2_1/c$
a (Å)	11.042(3)
b (Å)	13.631(3)
c (Å)	10.335(2)
α (°)	90
β (°)	95.607(4)
γ (°)	90
Z	4
D_x [Mg/m^3]	1.362
Crystal size [mm]	0.20 × 0.18 × 0.15
μ [mm^{-1}]	0.091
F(000)	664
Reflection collected/unique	8236/3140
Data/restraints/parameters	3140/0/217
θ Range for data collection [°]	2.38–26.38
R(int)	0.0424
Ranges of indices h, k, l	$-13 \le h \le 13$, $-17 \le k \le 16$, $-12 \le l \le 10$
Absorption correction	Multi-scan (T_{min} = 0.9821, T_{max} = 0.9865)
Final R indices [$I > 2\sigma(I)$]	R_1 = 0.0470, wR_2 = 0.1223
R indices (all data)	R_1 = 0.0824, wR_2 = 0.1457
Goodness of fit on F^2	0.999
$\Delta\rho$ (max/min) [e Å^{-3}]	0.230; −0.189

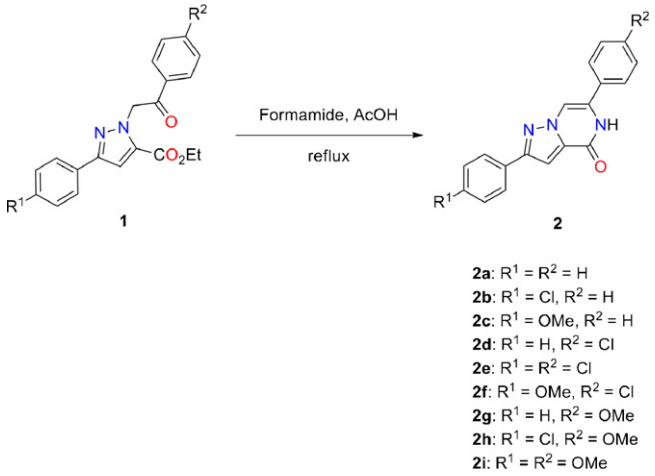

Scheme 1. Synthesis of 2,6-diphenylpyrazolo[1,5-*a*]pyrazin-4(5*H*)-ones.

3. Results and discussion

3.1. Synthesis

All synthesis of the 2,6-diphenylpyrazolo[1,5-*a*]pyrazin-4(5*H*)-ones **2** were followed the general pathway pictured in Scheme 1. Ethyl 1-(2-oxo-2-phenylethyl)-3-phenyl-1*H*-pyrazole-5-carboxylate derivatives **1** were prepared from 2-bromo-1-phenylethanone and ethyl 3-phenyl-1*H*-pyrazole-5-carboxylate derivatives as previously described [31]. Cyclization of **1** was achieved by modification of the literature procedure [32] to afford target compounds **2** in high yields. The structures of compounds **2** were in agreement with the molecular structures confirmed by spectroscopy including IR, ^{1}H NMR and HRMS spectra. The purity of these compounds was ascertained by TLC and spectral analysis.

A proposed cyclization mechanism involving a nucleophilic substitution was outlined in Scheme 2. In the reflux condition, formamide might first liberate NH_3 and the nucleophilic addition of NH_3 to the carbonyl carbon of ketone in compound **1** formed an imine intermediate (**A**) that should isomerize to an enamine (**B**) with more stable conjugated structure. A final irreversible lactamization of enamine (**B**) occurred rapidly and afforded target product. Similar to our previous report, the annulation reaction should be a tandem reaction of enamine formation and lactamization [33].

3.2. X-ray crystal structure

The molecular structure and atomic numbering scheme of compound **2c** is illustrated in Fig. 1. The molecular structure is dominated by the arrangement of the rings of the pyrazole, pyrazinone and two phenyls. In the pyrazinone group, the C9–O1, N1–C7, C7–C11 and N2–C11 bond lengths and all angles are comparable with similar literature values [33]. The C9–N1 distance 1.361(3) Å suggests some double-bond character due to the resonance delocalization of N-atom lone pairs with C9–O1 double-bond. The X-ray crystal structural research indicates that the compound **2c** adopts the keto form. The core pyrazolo[1,5-*a*]pyrazine fragment is essentially planar with maximum mean plane deviation of –0.021(2) Å for atom C11, and it is coplanar with the substituted benzene ring, with a dihedral angle of only about 3.00(4)°. The dihedral angle between the pyrazole ring and the unsubstituted phenyl ring is 25.40(6)°.

In the lattice of compound **2c**, the crystal structure are stabilized by π···π, C–H···π, N–H···O and C–H···N hydrogen bonds (Fig. 2 and Table 2). The orientation of the molecule enables the formation of a significant intramolecular hydrogen bond involving atom C15 and atom N3 and constitutes a five membered ring $S(5)$. Molecules are linked to form centrosymmetric dimers encoded as $R_2^2(8)$ by pairs of classical N–H···O hydrogen bonds, which are fairly short and almost linear. Molecules of **2c** are also stacked as cyclic dimer, as a result of pairs of *Cg*2···*Cg*4 interactions [*Cg*2···*Cg*4 = 3.727(15) Å, β = 22.58°, symmetry code: 2 − *x*, 1 − *y*, −*z*]. One aromatic π···π stacking interaction [*Cg*1···*Cg*1 = 3.4967(15) Å, β = 11.56°, symmetry code: 2 − *x*, 1 − *y*, −*z*] between pyrazole rings of the neighboring molecules also participates in supramolecular aggregation. In addition, an intermolecular interaction is observed between the atom C15 and the pyrazine ring with a distance of 3.757(2) Å.

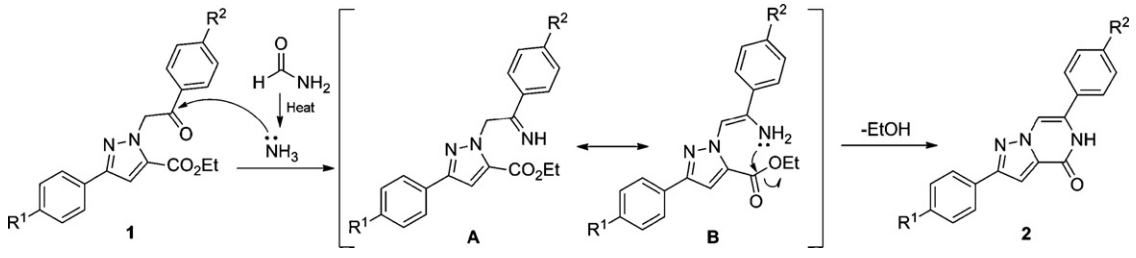

Scheme 2. Proposed mechanism for the synthesis of compounds **2**.

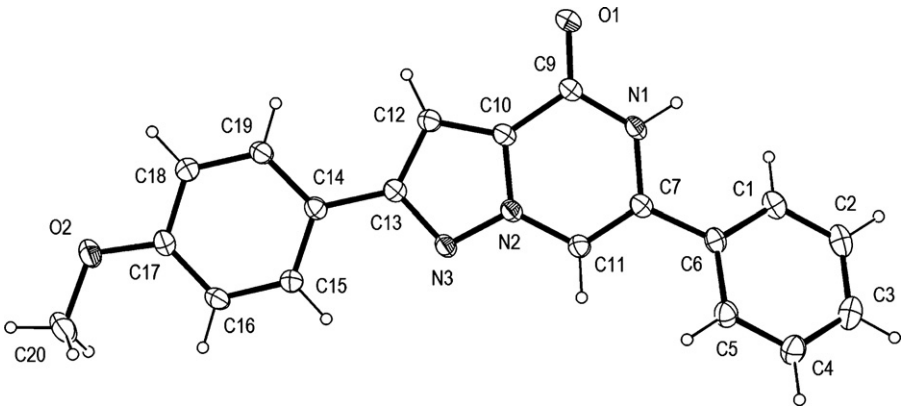

Fig. 1. ORTEP view of compound **2c**. Ellipsoids are represented at the 30% probability level.

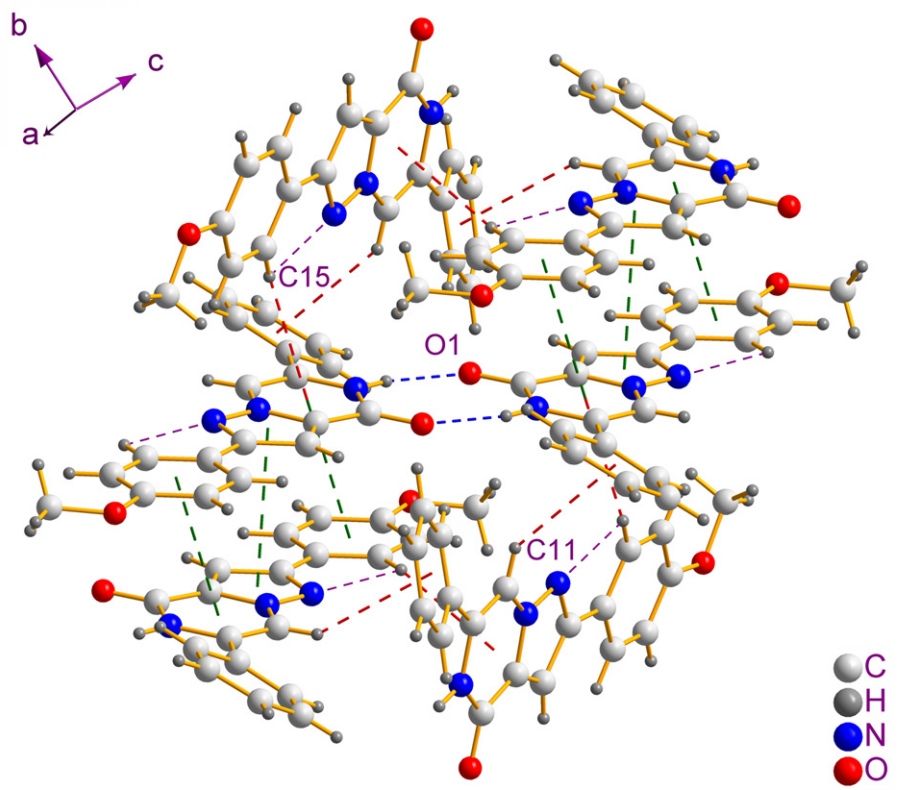

Fig. 2. Packing diagram of **2c**, showing hydrogen bonds and π···π interactions as dashed lines.

3.3. UV–vis absorption spectra

The UV–vis spectra of compounds **2a–i** were measured in THF solution at the concentration of 2.5×10^{-5} M and the results are listed in Table 3. As can be seen, all the compounds exhibit similar absorption spectra with maximum wavelengths of 285 nm (295 nm for compound **2b** and **2i**) and around 327 nm (Fig. 3). The first one is estimated as $\pi \rightarrow \pi^*$ transition of the enol form. The second absorption maxima are in connection with the $\pi \rightarrow \pi^*$ transition of the keto form with molar extinction coefficients ε values (10^4 M^{-1} cm^{-1}). It can be suggested that these compounds might exist in a mixture as keto and enol forms in THF solutions, due to the tautomerism in pyrazin-one structure. This keto–enol tautomerism involves a fast hydrogen transfer between nitrogen and oxygen and these compounds usually exist in the predominant keto form.

The electron-donating methoxy group (compounds **2c**, **2f**, **2g**, **2h** and **2i**), which increase the electron density by releasing electrons into the conjugated π-framework, affects the absorption spectra and produces bathochromic shifts ($\Delta\lambda_{max}$ = 2–3 nm). Also, it is

Table 2
Hydrogen bond geometry for compound **2c** (*Cg*1, *Cg*2, *Cg*3 and *Cg*4 are the centriods of pyrazole, pyrazine, benzene and substituted benzene ring, respectively).

D–H···A/π	D–H [Å]	H···A/π [Å]	D···A/π [Å]	D–H···A/π [°]
N1–H8···O1[a]	0.86	2.06	2.901(2)	167
C15–H15···N3	0.93	2.54	2.867(3)	101
C11–H11···*Cg*3[b]	0.93	2.95	3.745(2)	144
C15–H15···*Cg*2[b]	0.93	2.93	3.757(2)	149

Symmetry codes: [a] $2-x, 1-y, 1-z$; [b] $x, (1/2)-y, -(1/2)+z$.

Table 3
Physical properties of **2a–i**.

Compound	λ_{max} (nm)	ε_{max} (M^{-1} cm^{-1})	λ_{ex} (nm)	λ_{em} (nm)	Stock's shift (nm)	Φ_F
2a	325	1.21×10^4	329	389	60	0.48
2b	330	0.97×10^4	330	387	57	0.52
2c	327	1.18×10^4	331	390	59	0.50
2d	331	1.09×10^4	331	390	59	0.59
2e	330	1.31×10^4	329	392	63	0.55
2f	334	1.23×10^4	338	395	57	0.60
2g	327	1.34×10^4	331	396	65	0.57
2 h	329	1.15×10^4	330	394	64	0.52
2i	330	1.18×10^4	330	396	66	0.59

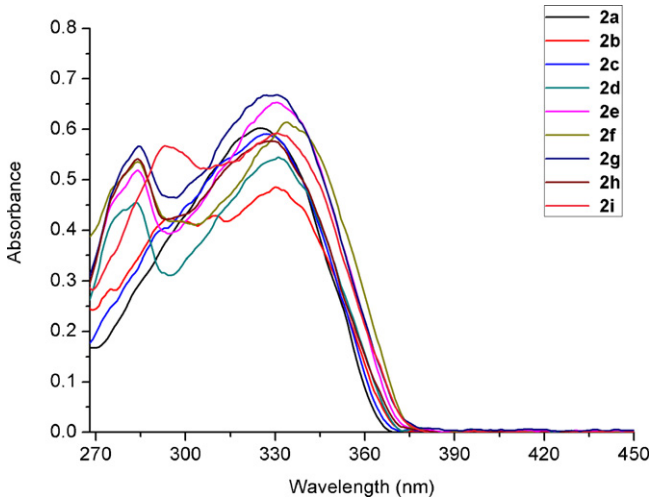

Fig. 3. UV–vis absorption spectra of **2a–i** in THF solution (2.5×10^{-5} M).

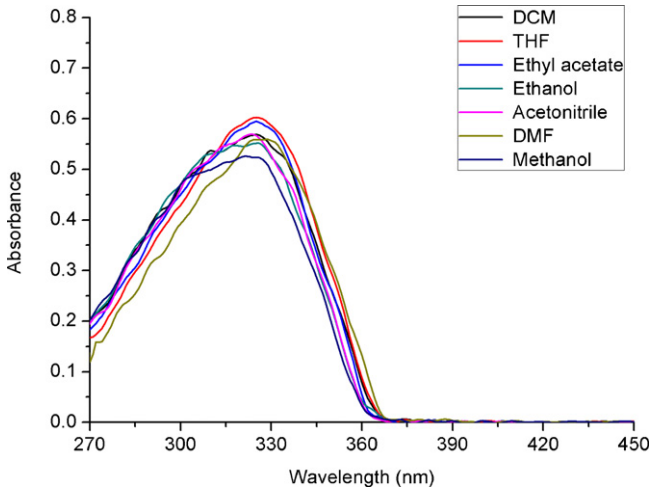

Fig. 4. UV–vis absorption spectra of compound **2a** taken at 2.5×10^{-5} M in different solvents.

interesting to note that the presence of hydrogen in R^2 position of the 2-phenyl moiety interfere the shapes of the absorption band of compounds **2a** and **2c**. The absorption spectra of compounds **2a** and **2c** show broad wavelength at 327 nm, which is well-overlapped with the absorption spectrum of the enol forms.

The UV–vis absorption spectra of the compound **2a** in dichloromethane, tetrahydrofuran, ethyl acetate, ethanol, acetonitrile and methanol are shown in Fig. 4. The UV–vis absorption spectra of compound **2a** in protic and aprotic solvents are little difference with respect to the absorption spectra in THF. It was observed that the absorption maxima of compound **2a** in aprotic solvents bathochromic shifted for about 5 nm with respect to the absorption spectra in methanol (λ_{max} = 318 nm). In other words, the absorption spectra of **2a** are dependent of solvent polarity although the effects are less. In aprotic solvents like DCM and ethyl acetate, the absorption spectra of **2a** have narrow bandwidths. However, the bandwidth increases in protic solvents such as methanol and ethanol with a slight decrease in absorbance. In general, spectral broadening is caused by the interactions between solutions and solute molecules [34].

Solvatochromism of the absorption is generally negligible, but the absorption is more sensitive towards the changes of alkalinity. The influence of pH on the absorption of the compound **2a** has been investigated by comparing the absorption maxima in methanol–H_2O (v/v = 1:1) medium with different pH (Fig. 5A). In the pH range from 1.63 to 8.04, the solution of compound **2a** has a lilac colour and displays a broad absorption maximum at the range 311–324 nm. For pH ≥8.56, the shapes and absorption max-

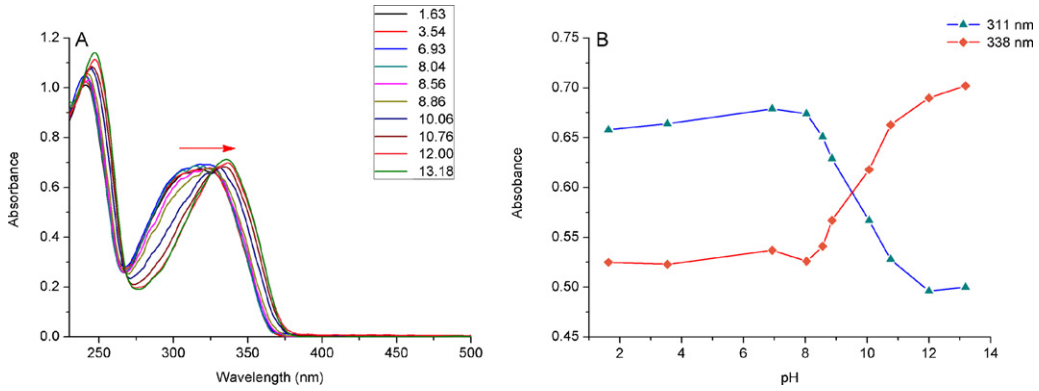

Fig. 5. UV–vis absorption spectra of **2a** at different pH (A), and effect of pH on UV–vis absorbance at 311 nm and 338 nm (B) in methanol–H_2O (v/v = 1:1) solutions.

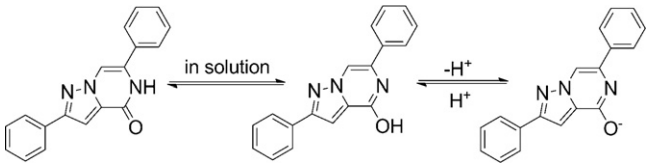

Scheme 3. Tautomeric forms and anionic form for **2a** in solution.

imum take place changes. With increasing of the alkalinity (pH 8.56–13.18), the characteristic absorption maximum for **2a** is obviously reduced and a new peak bathochromic shifted to 338 nm relative to neutral solution. In particular, the hyperchromism of the solution and the narrowing of absorption peak are observed. We speculate that such spectral transformations are caused by the deprotonation of the titled molecule (Scheme 3). The corresponding ionization constant pK_a determined by a spectrophotometric method [35] from the absorption spectra was about 9.7 (Fig. 5B).

Meanwhile, in order to get a further insight into the above mentioned changes, time-dependent density functional theory (TD-DFT) calculations were performed applying B3LYP/6–31G basis set to calculate excitation energies of compound **2a** in Gaussian 03 [36–38]. The frontier molecular orbitals and orbital energy levels of compound **2a** are shown in Fig. 6. The positive phase is red and the negative one is green.

Frontier molecular orbitals play important roles in the interactions between the molecules as well as in the electronic spectra of molecule. The energy gap between HOMO and LUMO determines the chemical reactivity, kinetic stability and optical polarizability of a molecule. In neutral solution, compound **2a** exists in keto and enol forms. As shown in Fig. 6, the electron density in the HOMO orbitals are localized at the pyrazolo[1,5-*a*]pyrazine skeleton in the two forms of compound **2a**. However, the LUMO orbitals are delocalized throughout the entire conjugated π-framework. Thus, the energy differences from HOMO to LUMO in the keto and enol are different (4.217 and 4.272 eV for keto and enol, respectively) due to their differences in LUMO energy levels. As a result of this, the broad absorption band of **2a** at 311–324 nm is assigned as combination of HOMO → LUMO transitions of keto and enol forms. Both of the HOMOs and LUMOs energy of keto and enol increase with the addition of alkali in compound **2a** solutions. As the HOMO increased much more, the HOMO–LUMO energy gap was calculated as 3.782 eV for the anionic form of compound **2a**, which is in agreement with the remarkable red shift in absorption spectra. All the results regarding pH effect on compound **2a** are consistent with the experimental findings.

3.4. Fluorescence

The photoluminescence spectra of compounds **2a**–**i** in THF solvent at excitation wavelength of 327 nm are presented in Fig. 7. The fluorescence emission maxima range from 387 to 396 nm. And that, the emission spectra of compounds **2a**–**i** showed two shoulders at the range of 365–384 nm and 401–418 nm. The shoulder emission may be due to the vibronic coupling that can undergo structural relaxation leading to different emitting conformation. Generally, for compounds **2a**–**i**, the vibrational structures of the

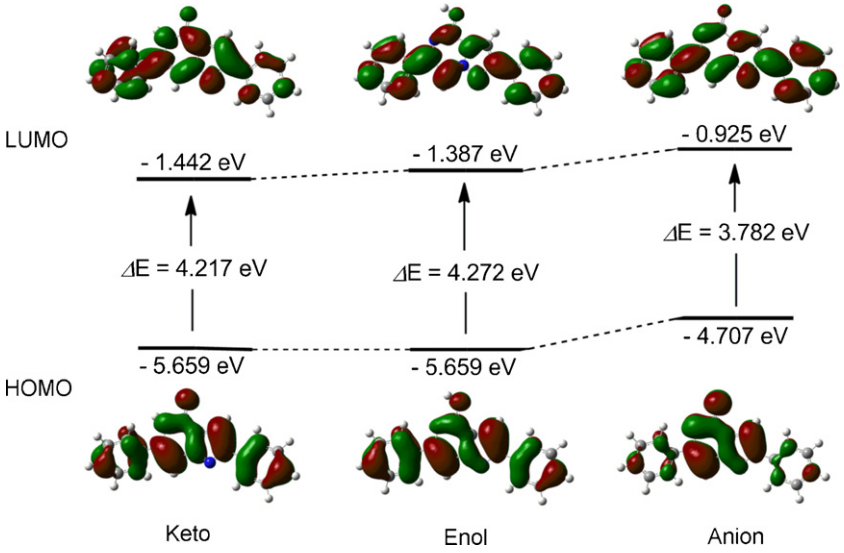

Fig. 6. HOMO and LUMO energy levels of compound **2a** for different forms.

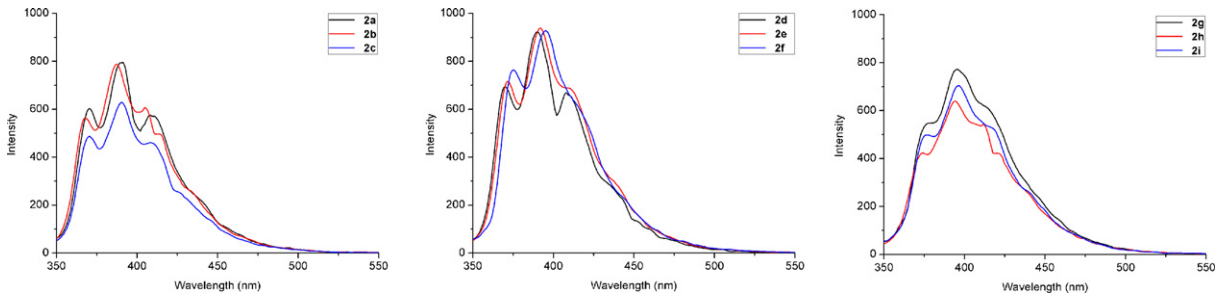

Fig. 7. The fluorescence spectra of the compounds **2a**–**i** in THF solution (2.0×10^{-7} M).

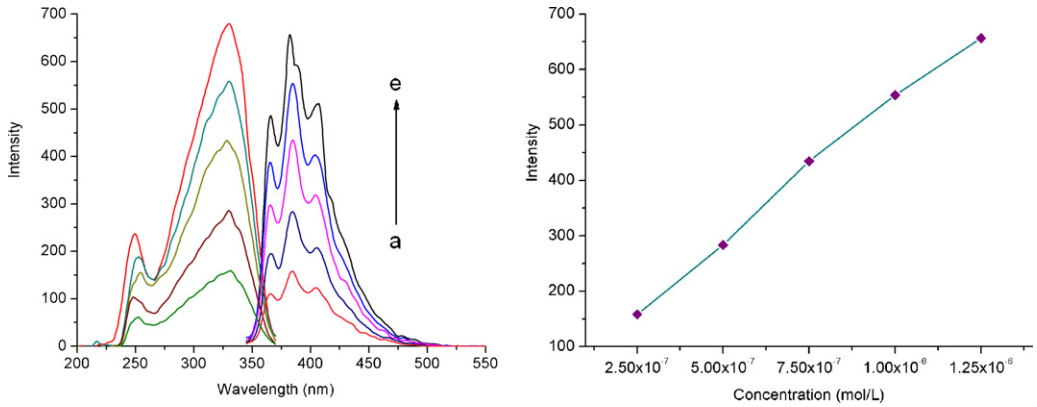

Fig. 8. Fluorescence spectra of compound **2a** in THF at different concentrations: (a) 2.5×10^{-7} M, (b) 5.0×10^{-7} M, (c) 7.5×10^{-7} M, (d) 1.0×10^{-6} M, (e) 1.25×10^{-6} M (excitation slit width 10 nm, emission slit width 2.5 nm).

fluorescence band are better than that of the absorption band. This kind of spectral behavior indicates a larger rigidity and planarity of the geometry of the emitting state (S_1) compared to that of the ground state (S_0) [39]. Compared with the compounds **2a–c**, compounds **2d–i** with chlorine or methoxy groups in the position R^2 cause a slight red shift in THF for 1–5 nm and 6–7 nm, respectively.

$$\Phi_F = \Phi_{ref} \frac{S_{sample} \cdot A_{ref} \cdot n^2_{sample}}{S_{ref} \cdot A_{sample} \cdot n^2_{ref}} \quad (1)$$

The fluorescence quantum yields of compounds **2a–i** in THF were calculated on the basis of the absorption and fluorescence spectra using Eq. (1) [40]. Where, Φ_F is quantum yield of sample, Φ_{ref} is quantum yield of quinine sulfate in 0.1 N H_2SO_4, A_{ref}, S_{ref}, n_{ref} and A_{sample}, S_{sample}, n_{sample} are the absorbance at the excited wavelengths, the integrated emission band area and the solvent refractive index of the standard and the sample, respectively. In most cases, the fluorescence quantum yields are found around 0.55 (Table 3).

The fluorescence behavior of compound **2a** at different concentrations in THF is shown in Fig. 8. On progressive increase in concentration of compound **2a**, the fluorescence intensity obeys Lambert–Beer law and the emission intensity increases linearly at lower concentrations. Deviations from Lambert–Beer law are not noticed at the concentration rang of 2.50×10^{-7} to 1.25×10^{-6} M.

We examined the fluorescence spectra of compound **2a** in seven solvents with different polarity and hydrogen bonding donor ability including methanol, acetonitrile, acetone, dixoane, tetrahydrofuran, dichloromethane and toluene. The results are listed in Table 4 and the representative fluorescence spectra are shown in Fig. 9. The fluorescence maxima and two shoulders are noteworthy in all solvents except methanol. In methanol, vibronic coupling can be hardly observed for compound **2a** due to the high polarity of the solvent. Also, changing the solvent does not largely alter the band positions. The greatest emission intensity in acetone is observed, while there is least emission intensity in methanol.

Table 4
Data of fluorescence spectra of compound **2a** in different solvents at the concentration of 2.0×10^{-7} M; λ_s is the fluorescence wavelength of the left 'shoulder'.

Solvent	λ_{ex} (nm)	λ_s (nm)	λ_{em} (nm)	Stoke's shift (nm)
Toluene	330	368	387	57
DCM	328	368	386	58
THF	332	370	390	58
Dioxane	332	367	386	54
Acetone	340	365	383	43
Acetonitrile	331	365	384	53
Methanol	328	–	388	60

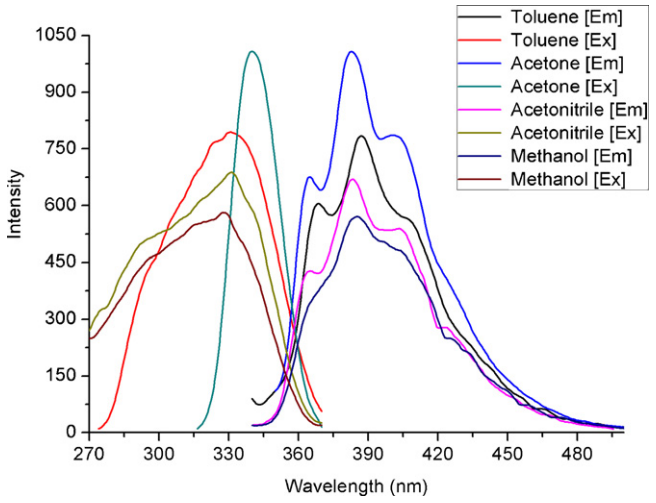

Fig. 9. The Fluorescence spectra of the compound **2a** in different solvents (2.0×10^{-7} M).

4. Conclusion

A series of 2,6-diphenylpyrazolo[1,5-*a*]pyrazin-4(5*H*)-ones were prepared and their structures were experimentally characterized by means of IR, ^{1}H NMR spectroscopy and typical compound **2c** was also determined by X-ray diffraction. The UV–vis absorption and fluorescence spectra of compounds **2a–i** in THF were observed to be similar. Moreover the spectra of representative compound **2a** in different solvents were studied and found that the solvent polarity had less effect. Furthermore, at alkaline solution condition compound **2a** presents in anion form to result in red shift of absorption maxima and these phenomena can be explained by calculative point of view. Also, fluorescence spectra of these compounds in THF and compound **2a** in several solvents are measured. The synthesized compounds displayed the interesting optical properties, which may promote their application as potential chemsensor.

Acknowledgements

This research was carried out with financial support from the National Natural Science Foundation of China (project nos. 90813022 and 20972088).

References

[1] I.J. Krems, P.E. Spoerri, Chem. Rev. 40 (1947) 279–358.
[2] T. Kosuge, H. Kamiya, Nature 193 (1962) 776.

[3] A. Ganesan, Angew. Chem. Int. Ed. 35 (1996) 611–615.
[4] S. Myadaraboina, M. Alla, V. Saddanapu, V.R. Bommena, A. Addlagatta, Eur. J. Med. Chem. 45 (2010) 5208–5216.
[5] M.J.C. Scanio, L. Shi, I. Drizin, R.J. Gregg, R.N. Atkinson, J.B. Thomas, M.S. Johoson, M.L. Chapman, D. Liu, M.J. Krambis, Y. Liu, C.C. Shieh, X.F. Zhang, G.H. Simler, S. Joshi, P. Honore, K.C. Marsh, A. Knox, S. Werness, B. Antonio, D.S. Krafte, M.F. Jarvis, C.R. Faltynek, B.E. Marron, M.E. Kort, Bioorg. Med. Chem. 18 (2010) 7816–7825.
[6] M. Abdel-Aziz, H.M. Abdel-Rahman, Eur. J. Med. Chem. 45 (2010) 3384–3388.
[7] Y.K.C. da Sliva, C.V. Augusto, M.L.C. Barbosa, G.M.A. Melo, A.C. de Queiroz, T.L.M.F. Dias, W.B. Júnior, E.J. Barreiro, L.M. Lima, M.S. Alexandre-Moreira, Bioorg. Med. Chem. 18 (2010) 5007–5015.
[8] M. Mosrin, T. Bresser, P. Knochel, Org. Lett. 11 (2009) 3406–3409.
[9] O. Shimomura, F.H. Johnson, Nature 256 (1975) 236–238.
[10] J.F. Head, S. Inouye, K. Teranishi, O. Shimomura, Nature 405 (2000) 372–376.
[11] R.I. Fonteriz, S. de la Fuente, A. Moreno, C.D. Lobatón, M. Montero, J. Alvarez, Cell Calcium 48 (2010) 61–69.
[12] M. Singh, S.E. Lofland, K.V. Ramanujachary, A. Ramanan, Cryst. Growth Des. 10 (2010) 5105–5112.
[13] B.J. Coe, J. Fielden, S.P. Foxon, I. Asselberghs, K. Clays, B.S. Brunschwig, Inorg. Chem. 49 (2010) 10718–10726.
[14] S. Takamizawa, E. Nataka, T. Akatsuka, R. Miyake, Y. Kakizaki, H. Takeuchi, G. Maruta, S. Takeda, J. Am. Chem. Soc. 132 (2010) 3783–3792.
[15] J.C. Chen, Q.H. Chen, Q. Guo, S. Ruan, H. Ruan, G.Q. He, Q. Gu, Food Chem. 122 (2010) 1247–1252.
[16] J.G. Pasipanodya, T. Gumbo, Antimicrob. Agents Chemother. 54 (2010) 2847–2854.
[17] N. Sugimoto, H. Watanabe, A. Ide, Tetrahedron 11 (1960) 231–233.
[18] G.M. Nitulescu, C. Draghici, A.V. Missir, Eur. J. Med. Chem. 45 (2010) 4914–4919.
[19] R. Kasımoğulları, M. Bülbül, B.S. Arslan, B. Gökçe, Eur. J. Med. Chem. 45 (2010) 4769–4773.
[20] C.S. Reddy, M.V. Devi, M. Sunitha, A. Nagaraj, Chem. Pharm. Bull. 58 (2010) 1622–1626.
[21] R. Manikannan, R. Venkatesan, S. Muthusubramanian, P. Yogeeswari, D. Sriram, Bioorg. Med. Chem. Lett. 20 (2010) 6920–6924.
[22] B.P. Bandgar, J.V. Totre, S.S. Gawande, C.N. Khobragade, S.C. Warangkar, P.D. Kadam, Bioorg. Med. Chem. 18 (2010) 6149–6155.
[23] Z.P. Yang, K. Zhang, F.B. Gong, S.Y. Li, J. Chen, J.S. Ma, L.N. Sobenina, A.I. Mikhaleva, B.A. Trofimov, G.Q. Yang, J. Photochem. Photobiol. A 217 (2011) 29–34.
[24] E. Koscien, J. Sanetra, E. Gondek, B. Jarosz, I.V. Kityk, J. Ebothe, A.V. Kityk, Spectrochim. Acta A 61 (2005) 1933–1938.
[25] B. Yang, Y. Lu, C.J. Chen, J.P. Cui, M.S. Cai, Dyes Pigments 83 (2009) 144–147.
[26] F. Karcı, N. Şener, M. Yamaç, İ. Şener, A. Demirçalı, Dyes Pigments 80 (2009) 47–52.
[27] E. Gondek, J. Nizioł, A. Danel, P. Szlachcic, K. Pluciński, J. Sanetra, I.V. Kityk, Spectrochim. Acta A 75 (2010) 1501–1505.
[28] R.A. Velapoldi, H.H. Tønnesen, J. Fluoresc. 14 (2004) 465–472.
[29] G.M. Sheldrick, Acta Crystallogr. A64 (2008) 112–122.
[30] A.L. Spek, Acta Crystallogr. D65 (2009) 148–155.
[31] L.W. Zheng, Y. Li, D. Ge, B.X. Zhao, Y.R. Liu, H.S. Lv, J. Ding, J.Y. Miao, Bioorg. Med. Chem. Lett. 20 (2010) 4766–4770.
[32] N. Micale, R. Ettari, T. Schirmeister, A. Evers, C. Gelhaus, M. Leippe, M. Zappalà, S. Grasso, Bioorg. Med. Chem. 17 (2009) 6505–6511.
[33] Y.S. Xie, H.L. Zhao, H. Su, B.X. Zhao, J.T. Liu, J.K. Li, H.S. Lv, B.S. Wang, D.S. Shin, J.Y. Miao, Eur. J. Med. Chem. 45 (2010) 210–218.
[34] B.L. van Duuren, Chem. Rev. 63 (1963) 325–354.
[35] N.U. Perišić-Janjić, A.A. Muk, V.D. Canić, Anal. Chem. 45 (1973) 798–801.
[36] P.J. Stephens, F.J. Devlin, C.F. Chabalowski, M.J. Frisch, J. Phys. Chem. 98 (1994) 11623–11627.
[37] W.J. Hehre, R. Ditchfield, J.A. Pople, J. Chem. Phys. 56 (1972) 2257–2261.
[38] P.A. Hariharan, J.A. Pople, Theor. Chim. Acta 28 (1973) 213–222.
[39] D.S. Karpovich, G.J. Blanchard, J. Phys. Chem. 99 (1995) 3951–3958.
[40] H. Shaki, K. Gharanjig, S. Rouhani, A. Khosravi, J. Photochem. Photobiol. A 216 (2010) 44–50.